DRAFT VERSION JANUARY 5, 2016
Preprint typeset using LaTeX style emulateapj v. 01/23/15

THE MASS OF THE BLACK HOLE IN THE X-RAY BINARY NOVA MUSCAE 1991

Jianfeng Wu[1], Jerome A. Orosz[2], Jeffrey E. McClintock[1], Imran Hasan[3], Charles D. Bailyn[3,4], Lijun Gou[5,6], Zihan Chen[5,6]

ApJ submitted

ABSTRACT

The optical counterpart of the black-hole soft X-ray transient Nova Muscae 1991 has brightened by $\Delta V \approx 0.8$ mag since its return to quiescence 23 years ago. We present the first clear evidence that the brightening of soft X-ray transients in quiescence occurs at a nearly linear rate. This discovery, and our precise determination of the disk component of emission obtained using our *simultaneous* photometric and spectroscopic data, have allowed us to identify and accurately model archival ellipsoidal light curves of the highest quality. The simultaneity, and the strong constraint it provides on the component of disk emission, is a key element of our work. Based on our analysis of the light curves, and our earlier measurements of the mass function and mass ratio, we have obtained for Nova Muscae 1991 the first accurate estimates of its systemic inclination $i = 43.2^{+2.1}_{-2.7}$ deg, and black hole mass $M = 11.0^{+2.1}_{-1.4}\ M_\odot$. Based on our determination of the radius of the secondary, we estimate the distance to be $D = 4.95^{+0.69}_{-0.65}$ kpc. We discuss the implications of our work for future dynamical studies of black-hole soft X-ray transients.

Subject headings: black hole physics — stars: black holes — binaries: general — X-rays: binaries

1. INTRODUCTION

Stellar-mass black holes are identified and studied in X-ray binary systems in the Milky Way and nearby galaxies (Remillard & McClintock 2006). The compact objects in two dozen of these systems are dynamically confirmed to be black holes with masses in the range $M = 5$–$30\ M_\odot$ (for the most recent review, see Casares & Jonker 2014). One remarkable property of the mass distribution of these black holes is the "mass gap", i.e., the lack of black holes with $M = 3-5\ M_\odot$ (e.g., Özel et al. 2010; Farr et al. 2011). Assuming that this mass gap is not caused by selection biases (e.g., Narayan & McClintock 2005), it provides an important constraint on supernova models (Fryer & Kalogera 2001; Belczynski et al. 2012; Kochanek 2014).

Mass measurements, along with estimates of distance D and systemic inclination i, have also made possible demonstrably reliable measurements of the spins of ten black holes via the continuum-fitting method (McClintock et al. 2014, and references therein). In turn, these spin measurements benefit a variety of astrophysical studies. For example, they are the basis for a correlation between jet power and black hole spin (Narayan & McClintock 2012; Steiner et al. 2013; McClintock et al. 2014; but also see Fender et al. 2010; Russell et al. 2013), which provides insights into the energy generation mechanism of relativistic jets (Narayan et al. 2014). In testing this correlation and its associated jet model, it is essential to increase the sample size, which is presently only five black-hole soft X-ray transients (which we refer to hereafter as BHSXTs). Especially important for the correlation is a single short-period BHSXT, A0620-00 ($P = 7.8$ hr), which anchors the correlation at low spin and low jet power. In this paper, we report estimates of M, i and D for Nova Muscae 1991 (GS/GRS 1124−683; hereafter NovaMus), another short-period BHSXT ($P = 10.4$ hr), which is very similar in many respects to A0620-00 (Remillard et al. 1992). The compact primary of NovaMus was dynamically confirmed to be a black hole shortly after its discovery by Remillard et al. (1992). Using our values of M, i and D for NovaMus, we will go on to estimate the black hole's spin (Chen et al. 2015) and test the jet model of Narayan & McClintock (2012) by comparing our spin estimate to the value predicted in Steiner et al. (2013).

In measuring the mass of a black hole in an X-ray binary, one must determine three parameters: 1) the value of the mass function $f(M)$, which sets a hard lower limit on the mass of the compact object; 2) the ratio of the mass of the secondary star to that of the black hole, $q \equiv M_2/M$; and 3) the orbital inclination angle i of the system. The first two parameters are usually obtained via spectroscopy in the optical or near-infrared (NIR) band. The value of the mass function is determined by the semi-amplitude of the radial velocity curve of the secondary K_2 and the orbital period P:

$$f(M) \equiv \frac{PK_2^3}{2\pi G} = \frac{M \sin^3 i}{(1+q)^2}. \quad (1)$$

It is relatively straightforward to determine q by measuring the rotational broadening of the photospheric lines $v \sin i$ (e.g., Wu et al. 2015). Usually, the greatest challenge is obtaining an accurate estimate of i, since none of the BHSXTs discovered to date exhibits an X-ray eclipse, as discussed by Narayan & McClintock (2005).

While estimates of i have been obtained for three BHSXTs by modeling jet data (e.g. Fender et al. 1999; Steiner & McClintock 2012; Steiner et al. 2012), the common approach to constraining i is to model multi-color optical/NIR light curves while the system is in X-ray quiescence. Ideally, during each orbital cycle the ellipsoidal light curve of the tidally-distorted secondary, which fills its Roche lobe, shows

jianfeng.wu@cfa.harvard.edu
[1] Harvard-Smithsonian Center for Astrophysics, 60 Garden Street, Cambridge, MA 02138, USA
[2] Department of Astronomy, San Diego State University, 5500 Campanile Drive, San Diego, CA 92182, USA
[3] Department of Astronomy, Yale University, P. O. Box 208101, New Haven, CT 06520, USA
[4] Yale-NUS College, 6 College Avenue East, Singapore, 138614
[5] National Astronomical Observatories, Chinese Academy of Sciences, Beijing 100012, China
[6] University of Chinese Academy of Sciences, Beijing 100012, China

two equal maxima and two unequal minima. A near-ideal example of such a light curve is that of GRO J1655−40 for which several groups have obtained estimates of *i* that are in good agreement (Orosz & Bailyn 1997; van der Hooft et al. 1998; Greene et al. 2001; Beer & Podsiadlowski 2002). In fact, GRO J1655−40 is the only BHSXT for which the error in the black hole mass is dominated by the uncertainties in the mass function and the mass ratio, rather than the uncertainty in *i* (Casares & Jonker 2014).

For most BHSXTs, however, the quiescent ellipsoidal optical/NIR light curves are contaminated by a non-stellar contribution from the accretion disk (and possibly the jet). This component, which can vary rapidly, often distorts the light curve, and it sometimes completely conceals the ellipsoidal modulation. This "disk-veiling" issue is most problematic for the short-period systems (defined here as P <12 hrs) which generally have relatively faint *K*- or *M*-type secondaries. Kreidberg et al. (2012) discuss three types of non-stellar optical/NIR emission. One is a constant "pedestal" level of emission from the disk that dilutes the amplitude of the ellipsoidal modulation. The second is a component that varies periodically with the orbital period of the system, producing asymmetric distortions in the light curves, thereby increasing or decreasing the amplitude of the ellipsoidal-component of modulation. We model this component as emission from a wedge-shaped hotspot on the disk. These two disk components of light can be included in the light-curve model.

In addition, there is a third and more problematic component, namely, aperiodic flickering due to variability in the accretion flow. Cantrell et al. (2008) elucidated this component by identifying two principal distinct optical state for A0620−00 in quiescence, the *passive* and *active* states. Cantrell et al. concluded that only light curves in the passive state, which have minimal aperiodic variability, are suitable for modeling in order to estimate *i*; those in the active state are dominated by aperiodic flickering and are unsuitable. Cantrell et al. also found that A0620−00 in the active state is brighter than in the passive state by by ~ 0.3 mag, which is expected as the accretion disk "builds up" during quiescence (Lasota 2001). Kreidberg et al. (2012) further investigated the potential systematic uncertainties of using active-state data in estimating *i* and *M*.

In summary, accurate measurements of *i* and *M* for BHSXTs requires that one selects and models light curves obtained in the passive quiescent state. Even in this case, careful modeling of the pedestal and hotspot components is required; this is particularly true in the case of the short-period systems, such as A0620–00 and NovaMus. However, in most earlier studies of BHSXTs, the disk contribution was only crudely estimated, or it was ignored altogether, while no distinctions were drawn between passive- and active-state data. Consequently, in a number of cases, there has been wide disagreement in the inclination estimates that have been obtained for the same system (see summary in Table 1 of Casares & Jonker 2014).

Earlier studies of NovaMus have provided estimates of $f(M)$, q, i, and M (e.g., Orosz et al. 1996; Casares et al. 1997; Gelino et al. 2001). However, in no case has the disk contribution to the optical/NIR light curves been robustly constrained. In the most recent work, Gelino et al. (2001) obtained an estimate of $i = 54^\circ \pm 1.5^\circ$ by modeling the *J* and *K* band light curves assuming that the disk contribution is negligible, an assumption that was subsequently shown to be ill-founded (Reynolds et al. 2008; Kreidberg et al. 2012). Based on the mass measurement of Gelino et al., Morningstar et al. (2014) found a retrograde spin ($a_* = -0.25^{+0.05}_{-0.64}$) for the black hole in NovaMus, which is a remarkable result for a black hole in a BHSXT, given that the spin of the black hole is believed to be accrued gradually over the lifetime of the system via accretion torques (Fragos & McClintock 2015).

In this work, we present the first accurate measurements of the inclination of the binary system and the mass of the black hole, as well as an estimate of distance. The accuracy of our results derives from (i) the unprecedented quality of our determination of the disk veiling and the quality of our radial velocity data; (ii) use of the first reliable measurement of the mass ratio q; and (iii) the exclusive use of passive light-curve data in modeling the ellipsoidal variability, namely, data obtained shortly after the system returned to quiescence following its 1991 outburst (Orosz et al. 1996). In our earlier paper on the dynamics of NovaMus (Wu et al. 2015, hereafter Paper I), we extensively discuss items (i) and (ii). Meantime, item (iii) is a feature topic of this work (§2.2).

As elaborated in Paper I, in 2009 we tackled the problem of the variable component of non-stellar emission by making phase-resolved spectroscopic and photometric observations of NovaMus that were strictly simultaneous (< 1 s). The spectroscopic and photometric data were both collected at Las Campanas Observatory using the Magellan/Clay 6.5 m and du Pont 2.5 m telescopes, respectively. We obtained 72 high-resolution spectra using the Magellan Echellette spectrograph (MagE; Marshall et al. 2008), which cover the wavelength range 3000–10000 Å. Based on independent measurements for several echellette orders, we obtained the following precise and robust results: $K_2 = 406.8 \pm 2.7$ km s^{-1} and $v \sin i = 85.0 \pm 2.6$ km s^{-1}, which respectively imply $f(M) = 3.02 \pm 0.06\, M_\odot$ and $q = 0.079 \pm 0.007$. Of paramount importance for this work in modeling the light curves, we obtained a precise constraint on the fraction of the light due to the disk in 2009: $56.7 \pm 1.4\%$ in the V-band.

In this work, we use the results described above from Paper I to model the multi-color light curves of NovaMus in order to obtain reliable estimates of M, i, D, and other parameters for NovaMus. The structure of this paper is as follows. In §2, we first document the steady brightening of NovaMus during quiescence. Then, from all available data, we select the light curves that are suitable to model, and for each light curve we constrain the fraction of the light contributed by the disk. In §3 we detail the procedures we use to model the data, and we present the final adopted values of M and i, and all other model parameters. In §4 we estimate the distance to NovaMus, a parameter that is crucial for measuring the spin via the continuum-fitting method. Our summary and discussion are presented in §5.

2. PHOTOMETRIC DATA

2.1. *Optical Brightening of NovaMus during X-ray Quiescence*

The V-band light curve we obtained in 2009 contains a strong and variable, non-stellar component of light (Paper I), and it is grossly inferior for ellipsoidal modeling compared to the passive-state light curves obtained in 1992–1993 by Orosz et al. (1996). Furthermore, the system was 0.65 mag brighter in V in 2009 than it was in 1992–1993. These results motivated us to investigate how NovaMus brightened during this period, whether regularly and gradually, or chaotically.

Long-term photometric monitoring of NovaMus in X-ray

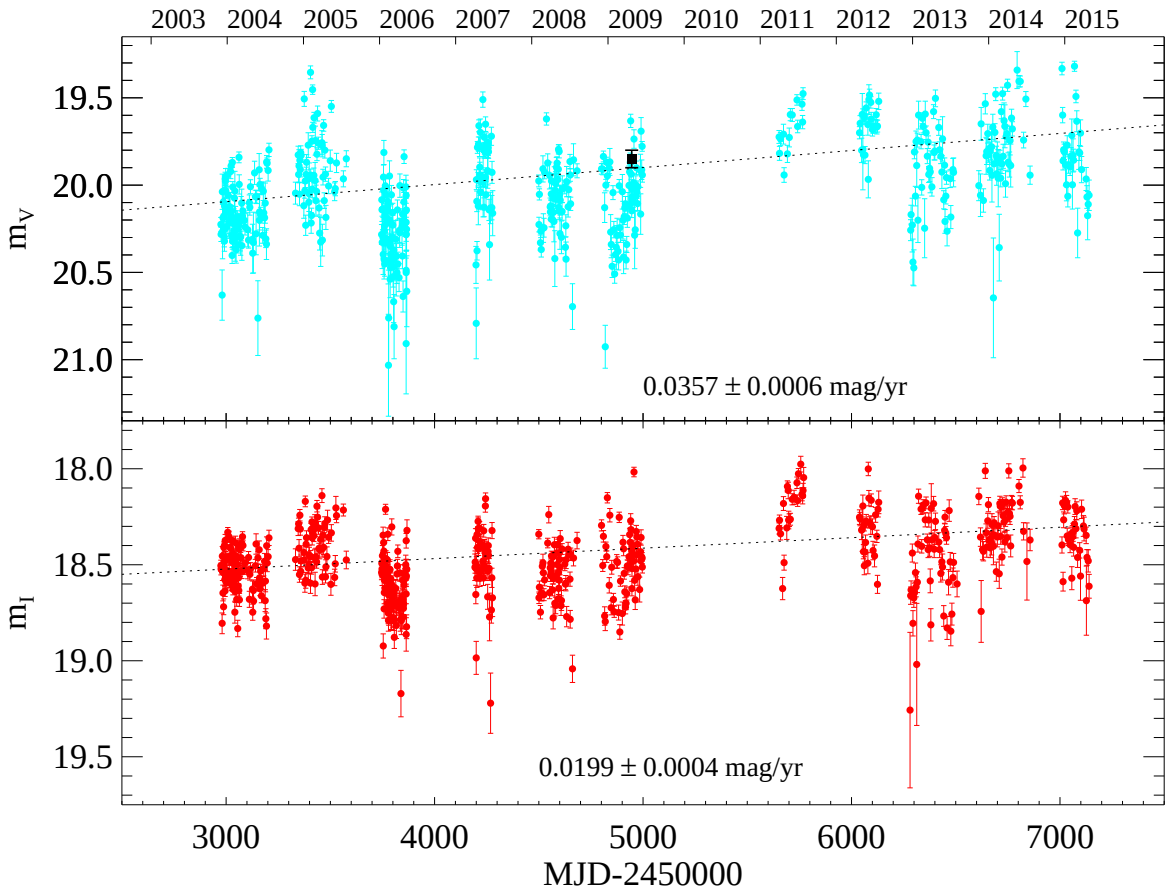

FIG. 1.— SMARTS light curves of NovaMus for the period 2003–2015 in the V-band (upper panel; filled cyan circles) and in the I-band (lower panel; filled red circles). The dashed line and rate of brightening given in each panel are the result of a linear fit to the data. The filled black square represents our mean V-band magnitude of NovaMus obtained in 2009 with the du Pont telescope.

quiescence has been performed on a near-nightly basis using the Small and Moderate Aperture Research Telescope System (SMARTS)[7]. We made use of the V- and I-band photometric data for the years 2003–2015, sans 2010. The data set comprises 556 frames in the V band and 592 frames in the I band (Fig. 1). We performed differential photometry using nearby, calibrated standard stars with $V-I$ colors similar to those of NovaMus. Our estimates of photometric error (shown in Fig. 1), which are statistical, are typically ~ 0.05 mag for the V-band and ~ 0.04 mag for the I-band. Our estimate of the uncertainty in the zero point for each band is ~ 0.05 mag.

Fig. 1 shows for both bands a clear trend of brightening of NovaMus over the course of 12 years. Applying a least-square linear regression to all the data points, we find that NovaMus brightened at a rate of 0.0357 ± 0.0006 mag yr^{-1} in the V-band and 0.0199 ± 0.0004 mag yr^{-1} in the I-band. *This is the first direct evidence of a gradual and a near-linear brightening of a BHSXT during X-ray quiescence.* It is worth noting that the rate of brightening is greater in the V-band than the I-band; i.e., the pedestal of disk emission becomes bluer as the system brightens. This may be caused by an increase in the temperature of the disk, or by a change in the structure of the disk (e.g., a decrease in the inner-disk radius).

[7] `http://www.astro.yale.edu/smarts`.

The brightening is predicted by the disk instability model (DIM; for a review see Lasota 2001). According to the DIM, and as these light curves show, after its return to quiescence following an outburst the disk of a BHSXT slowly but steadily builds via accretion, and the system brightens as the pedestal component grows (see Fig. 3 of Dubus et al. 2001). Meanwhile, the DIM does not predict the growth of aperiodic flickering and the distortions that develop in the ellipsoidal light curves as the quiescent system transitions from the passive optical state to the active state (Cantrell et al. 2008). According to the DIM, eventually a disk instability is triggered and a new outburst begins when the surface density of the disk at some radius reaches a critical value. The outburst recurrence time for BHSXTs can be years or decades. NovaMus has remained in quiescence for 24 years, ever since its only known outburst in 1991. By including disk irradiation and truncation into the instability model, while modeling the inner accretion flow as an advection dominated accretion flow (ADAF; Narayan & Yi 1994), Dubus et al. (2001) reproduced the long recurrence times for BHSXTs.

2.2. *Selection of Light Curves*

As discussed above, only light curves obtained in the passive state are useful in attempting to constrain the inclination. Unfortunately, the high-quality V-band data we obtained in 2009 using the du Pont telescope are unsuitable because No-

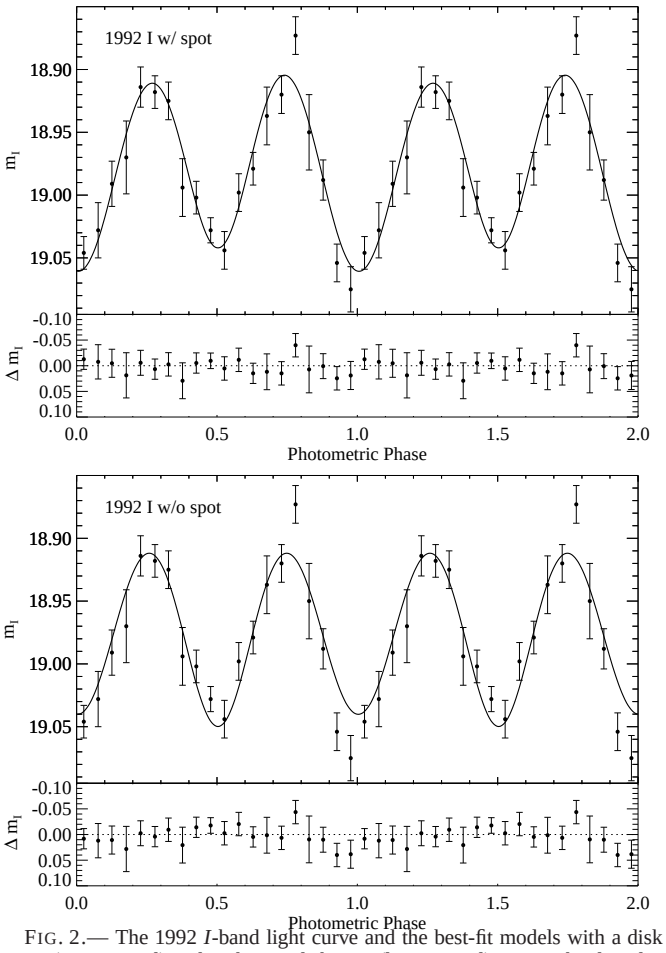

FIG. 2.— The 1992 *I*-band light curve and the best-fit models with a disk spot (upper panel) and without a disk spot (lower panel). Two orbital cycles are plotted for clarity.

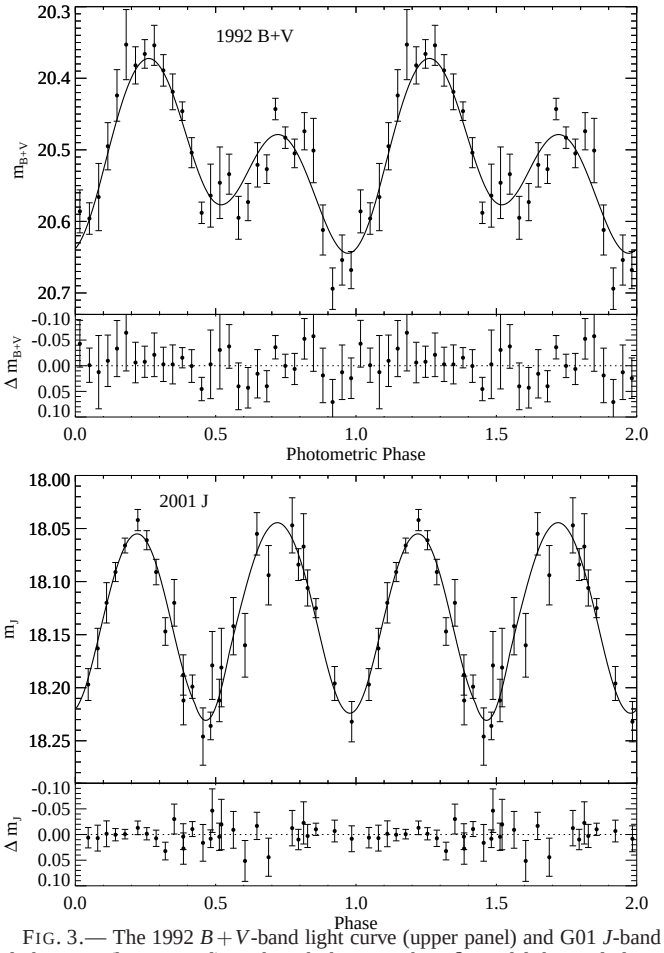

FIG. 3.— The 1992 $B+V$-band light curve (upper panel) and G01 *J*-band light curve (lower panel), each with their own best-fit model that includes a disk spot. Two orbital cycles are plotted for clarity.

vaMus was in an active state, as evidenced by strong aperiodic flickering (see Fig. 8 of Paper I). Likewise, the SMARTS light curves are dominated by aperiodic variations, showing that NovaMus has been in an active state since at least 2003. Therefore, the du Pont and SMARTS light curves cannot be expected to provide reliable constraints on the inclination.

We therefore turned to examine the highest-quality archival light curves in the literature, namely, those of Orosz et al. (1996) and Gelino et al. (2001), while passing over the *H*-band light curve of Shahbaz et al. (1997) because of its less desirable quality. We first discuss the light curves of Orosz et al. (1996). They were obtained in 1992–1995, shortly after the 1991 outburst of NovaMus, and they are thus minimally contaminated by disk emission. The authors present light curves in two bands: a $B+V$-band and a wide *I*-band, which have central wavelengths of ≈ 5000 Å and ≈ 9000 Å, respectively. Orosz et al. report that in 1992 NovaMus had a *V*-band magnitude of 20.51 ± 0.07, which was fainter than we observed in 2009 by 0.66 ± 0.09 mag. Based on these two data points, the average rate of brightening for the 17-year period 1992–2009 is 0.0388 ± 0.0053 mag yr^{-1}, which is consistent with the rate of 0.0357 ± 0.0006 mag yr^{-1} determined using SMARTS data for 2003–2015 (§2.1).

The 1992 wide *I*-band light curve (see Fig. 2) of Orosz et al. (1996) appears most desirable because it is least affected by aperiodic flickering. Meanwhile, we also choose to model the $B+V$-band light curve (see upper panel of Fig. 3), which was obtained during the same year, even though it is distorted, presumably by emission from a spot on the disk (see §1). We further selected the *J*-band light curve of Gelino et al. (2001), which appears to be relatively free of aperiodic variations and dominated by ellipsoidal modulation, while ignoring their relatively poor quality *K*-band light curve.

TABLE 1
FRACTION OF DISK EMISSION FOR THREE LIGHT CURVES

Light Curve	Mean *V*-band Magnitude	Disk Fraction (%)	
		V-band	*I*-band
2009 *V*	19.85 ± 0.05	56.7 ± 1.4	42.1 ± 2.8
1992 $B+V$, *I*	20.51 ± 0.07	$20.5^{+6.1}_{-6.6}$	$12.5^{+4.2}_{-4.3}$
2001 *J*	20.83 ± 0.45	< 29.5	< 18.8

2.3. *Constraining the Fraction of Disk Emission*

Although simultaneous spectroscopic data were not obtained for our selected light curves, we are still able to constrain the fraction of disk emission (referred to hereafter as the disk fraction) using the results derived from our simultaneous spectroscopic/photometric campaign in 2009 presented in Paper I. Following Cantrell et al. (2010), we make the reasonable assumption that the flux from the secondary star remains constant, and that the change in brightness of the system orig-

TABLE 2
LIST OF ELC MODEL PARAMETERS

Parameter	Lower Bound	Upper Bound	Definition (unit)
i	30	80	Inclination (deg)
K_2	395	420	Radial velocity semi-amplitude of the secondary (km s^{-1})
M_2	0.3	1.5	Mass of the secondary ($M_\odot$)
$\Delta\phi$	-0.015	0.015	Phase shift (deg)
$r_{\rm out}$	0.300	0.999	Radius of the outer rim of the accretion disk[a]
$\beta_{\rm rim}$	0.5	22.5	Opening half-angle of the disk rim (deg)
$T_{\rm disk}$	3000	49000	Temperature of the inner rim of the disk (K)
ξ	-0.99	-0.10	Power-law index of the disk temperature profile
$s_{\rm spot}$	0.6	15	The scale applied to obtain the disk spot temperature
$r_{\rm cut}$	0.05	1.0	Cut-off radius of the disk spot[b]
$\theta_{\rm spot}$	0	360	Azimuth of the disk spot (deg)
$w_{\rm spot}$	3	90	Angular size of the disk spot (deg)
M	···	···	Mass of the black hole ($M_\odot$)
K_1	···	···	Radial velocity semi-amplitude of the Black Hole (km s^{-1})
$\log g_2$	···	···	Surface gravity of the secondary (cm s^{-2})
R_2	···	···	Radius of the secondary ($R_\odot$)
a	···	···	Separation between the centers of the black hole and the secondary ($R_\odot$)
$v\sin i$	···	···	Rotational Velocity of the secondary (km s^{-1})

NOTE. — The first set of parameters and their bounds are fit parameters, and the second set are derived parameters.
[a] In units of the effective Roche lobe radius of the black hole.
[b] In units of the disk radius.

inates solely from the accretion disk.

During our 2009 observations, the mean V magnitude of NovaMus was 19.85 ± 0.05, with the accretion disk contributing $56.7 \pm 1.4\%$ of the total light (Paper I). This implies a magnitude for the secondary star alone of $m_{\rm V} = 20.76 \pm 0.06$. During 1992, the mean V magnitude of NovaMus was 20.51 ± 0.07 (Orosz et al. 1996), just 0.25 ± 0.09 mag brighter than the star alone. Thus, in 1992 the disk fraction was only $20.5^{+6.1}_{-6.6}\%$ (Table 1).

With these V-band results in hand, we estimated the disk fraction for the I-band using the spectral energy distribution model presented in §4.2 of Paper I. The model assumes a blackbody spectrum with an effective temperature of 4400 K for the stellar component and a power-law spectrum for the disk component (see Fig. 7 of Paper I). Extrapolating the power-law component, we obtain for 1992 a disk fraction of $12.5^{+4.2}_{-4.3}\%$ in the I-band.

Using the same procedure, we estimated the disk fraction for the 2001 J-band light curve (Table 1). However, in this case we only have a crude estimate of the mean V-band magnitude of NovaMus because Gelino et al. (2001) report just a single measurement of V-band magnitude, 20.83 ± 0.06, with no time-stamp. Thus, the orbital phase of the observation is unknown, and we therefore adopt an uncertainty of $\Delta m_{\rm V} = 0.45$ mag, i.e., the full amplitude of the 2009 V-band light curve. Using this magnitude and our model, we constrain the disk fractions in the V- and I-bands in 2001 to be $< 29.5\%$ and $< 18.8\%$, respectively. The J-band disk fraction is computed separately using a stellar-atmosphere model during the modeling of the light curve, which is described in the next section.

3. DYNAMICAL MODELING

3.1. *Description of the Eclipsing Light Curve Model*

In constraining the inclination i of NovaMus, we model our three selected light curves using the Eclipsing Light Curve (ELC; Orosz & Hauschildt 2000) code. The ELC code generates model light curves that include contributions from both the secondary star and the accretion disk, including an allowance for emission from a hot spot on the disk. The secondary star is assumed to be in a circular orbit, rotating synchronously, and filling its Roche lobe. We fix the effective temperature of the secondary to be $T_2 = 4400 \pm 100$ K based on the results of our cross correlation analysis (see §3.1 and Fig. 2 of Paper I); meanwhile our ELC models are insensitive to the adopted value of T_2. We ignore X-ray heating because the quiescent X-ray luminosity of NovaMus is minuscule ($L_{\rm X} \sim 4 \times 10^{31}$ erg s^{-1}; Sutaria et al. 2002).

The fit and derived parameters of the ELC models are listed in Table 2. There are four key fit parameters: the inclination i, K-velocity of the secondary K_2, mass of the secondary M_2 and a relative phase shift $\Delta\phi$. Our measured values of K_2 ($= 406.8 \pm 2.7$ km s^{-1}) and $v\sin i$ ($= 85.0 \pm 2.6$ km s^{-1}) reported in Paper I are used to generate the prior probability distribution for each of the four parameters. The posterior probability distribution of the parameters generated by the ELC code are required to agree closely with the measured values, which serves as a consistency check on the modeling process. We fix the orbital period to be $P = 0.43260249(9)$ d (Table 2 of Paper I).

There are four additional fit parameters that characterize the emission from the accretion disk: 1) the radius of the outer rim of the disk $r_{\rm out}$, expressed in units of the effective Roche lobe radius of the primary (Eggleton 1983); 2) the half opening angle of the accretion disk $\beta_{\rm rim}$; 3) the temperature of the inner edge of the disk $T_{\rm disk}$; and 4) the power-law index of the temperature profile along the disk radius ξ. For those models that include a hotspot along the outer rim of the accretion disk, there are four additional fit parameters: $s_{\rm spot}$ (the scaling factor used to derive the spot temperature from the disk temperature); $r_{\rm cut}$ (the inner cut-off radius of the spot); $\theta_{\rm spot}$ (the azimuth of the disk spot relative to the line connecting the center of the primary and secondary); and $w_{\rm spot}$ (the angular width of the disk spot).

For each fit parameter, we set a range of physically and/or geometrically reasonable values (see Table 2), some of which

TABLE 3
BEST-FIT PARAMETERS OF ELC MODELS

Parameter	1992 I		1992 $B+V$ and I	2001 J
	w/ spot	w/o spot		
i (deg)	$43.2^{+2.1}_{-2.7}$	$40.5^{+2.3}_{-2.5}$	$40.7^{+3.4}_{-2.8}$	$40.8^{+6.1}_{-2.6}$
K_2 (km s^{-1})	$407.0^{+2.1}_{-2.3}$	$406.9^{+2.3}_{-2.2}$	$406.6^{+2.2}_{-1.8}$	$406.5^{+2.5}_{-1.7}$
M_2 ($M_\odot$)	$0.89^{+0.18}_{-0.11}$	$1.05^{+0.21}_{-0.15}$	$1.03^{+0.26}_{-0.16}$	$1.02^{+0.21}_{-0.28}$
$\Delta\phi$	$0.006^{+0.008}_{-0.007}$	$0.003^{+0.010}_{-0.009}$	>0.007	<0.008
$r_{\rm out}$	0.58[a]	... [b]	>0.40	>0.76
$\beta_{\rm rim}$ (deg)	$6.4^{+5.8}_{-1.9}$	10.7	>13.4	>13.2
$T_{\rm disk}$ (10^4 K)	<1.77	>0.37	<1.49	>0.80
ξ	$-0.69^{+0.37}_{-0.12}$	>-0.68	$-0.45^{+0.17}_{-0.22}$	$-0.76^{+0.27}_{-0.11}$
$s_{\rm spot}$	>3.3	... [c]	>3.9	>3.4
$r_{\rm cut}$	<0.26	... [c]	<0.37	$0.35^{+0.06}_{-0.26}$
$\theta_{\rm spot}$ (deg)	10^{+29}_{-26}	... [c]	304^{+7}_{-15}	74^{+6}_{-15}
$w_{\rm spot}$ (deg)	17^{+20}_{-12}	... [c]	<26	33^{+14}_{-15}
M ($M_\odot$)	$11.0^{+2.1}_{-1.4}$	$12.9^{+2.2}_{-1.7}$	$12.7^{+3.1}_{-1.8}$	$12.6^{+2.4}_{-3.5}$
K_1 (km s^{-1})	$32.8^{+2.5}_{-1.9}$	$33.0^{+2.5}_{-2.4}$	$33.0^{+2.4}_{-2.3}$	32.8 ± 2.3
$\log g_2$ (cm s^{-1})	$4.34^{+0.03}_{-0.02}$	$4.36^{+0.03}_{-0.02}$	4.36 ± 0.03	$4.36^{+0.03}_{-0.05}$
R_2 ($R_\odot$)	$1.06^{+0.07}_{-0.04}$	$1.12^{+0.07}_{-0.05}$	$1.11^{+0.09}_{-0.06}$	$1.11^{+0.07}_{-0.11}$
a ($R_\odot$)	$5.49^{+0.32}_{-0.24}$	$5.79^{+0.32}_{-0.26}$	$5.76^{+0.44}_{-0.29}$	$5.75^{+0.35}_{-0.60}$
$v\sin i$ (km s^{-1})	$84.8^{+2.3}_{-1.9}$	$84.9^{+2.3}_{-2.2}$	$84.9^{+2.3}_{-2.2}$	84.7 ± 2.2
χ^2_ν (ν)	1.03 (8)	1.10 (12)	0.88 (38)	0.84 (17)

NOTE. — The quoted uncertainties or upper/lower limits are at the 1σ level of confidence.
[a] The quoted value corresponds to the model with minimum χ^2. However, no meaningful uncertainty range can be given because the χ^2 curve is flat.
[b] Parameter is unconstrained in the absence of a spot.
[c] These spot parameters are irrelevant for this model.

are based on the results in Paper I. For each set of trial values of the parameters, and for a particular filter band, the ELC code generates a model light curve. The observed light curves are fitted to the model curves using a variety of optimizing techniques (see details in §5.2.1 of Orosz et al. 2014). After a large number of trials, the model giving the global minimum χ^2 is adopted. Other systemic parameters, such as the black hole mass M and the radius of the secondary R_2, are derived using this best-fit model (see Table 2).

3.2. *Light Curve Fitting*

As already indicated in §2.2, among the three selected light curves the 1992 I-band light curve appears to be the most favorable: it is weakly affected by aperiodic flickering, its disk fraction is minimal ($\approx 12.5\%$), and it is much less distorted than its companion $B+V$-band curve. Compared to the 2001 J-band light curve, the constraint on the disk fraction for the I-band light curve is tighter and the disk was significantly fainter in 1992 (~ 0.3 mag; §2.1). We therefore choose the 1992 I-band light curve as our primary data set.

We generated a total of 2.5 million model light curves using the ELC code for the 1992 I-band data. The models include emission from the secondary star and from the disk, which is comprised of a steady component and a periodically variable component due to a hotspot. The model light curve that yields the minimum χ^2 is identified. The corresponding fit parameter values are listed in the second column of Table 3. For all 2.5 million models, we plotted the parameter value vs. $\Delta\chi^2$. In Figs. 4 and 5, we show respectively for the fit parameters and the derived parameters only the outer envelope defined by the mass of points. The three dashed lines shown in each panel correspond to $\Delta\chi^2 = 1, 4, 9$. The points of intersection of these lines with the envelope define respectively the 1σ, 2σ, 3σ uncertainty range of the parameter in question. For some fit parameters (e.g., $T_{\rm disk}$) there is only a one-sided constraint; in these cases, in Table 3 we quote 1σ lower/upper limits.

For our primary data set, the 1992 I-band light curve, the observed and model light curves, and fit residuals, are shown in the upper panel of Fig. 2. The model curve is itself shown decomposed into contributions from the secondary and from the disk in the top panel of Fig. 6. As this figure makes clear, both the constant and variable components of disk emission are relatively unimportant.

We also fitted the 1992 I-band light curve with models with no hotspot component. The values of the fit parameters, which are given in the third column of Table 3, are in good agreement with those obtained for the model that includes a spot. However, the quality of the fit is significantly poorer, as shown by an inspection of the fit residuals, which show evidence of modulation at the orbital period (lower panel of Fig. 2).

We further fitted the 1992 $B+V$-band and I-band light curves jointly, and the 2001 J-band light curve, including the hotspot in both cases, and we find results that are consistent with those obtained for our primary data set. The results are listed in the fourth and fifth columns of Table 3, respectively. The disk fractions we used (including both the constant and hotspot emission) are those given in Table 1. In both cases, the best-fit parameters are consistent with those obtained for our primary data set, the 1992 I-band light curve. Furthermore, in all cases the values of K_2 and $v\sin i$ returned by the models agree well with our measured values given in Paper I. Thus, the fit results for all three light curves are consistent, and the models in all cases are in good agreement with our dynamical

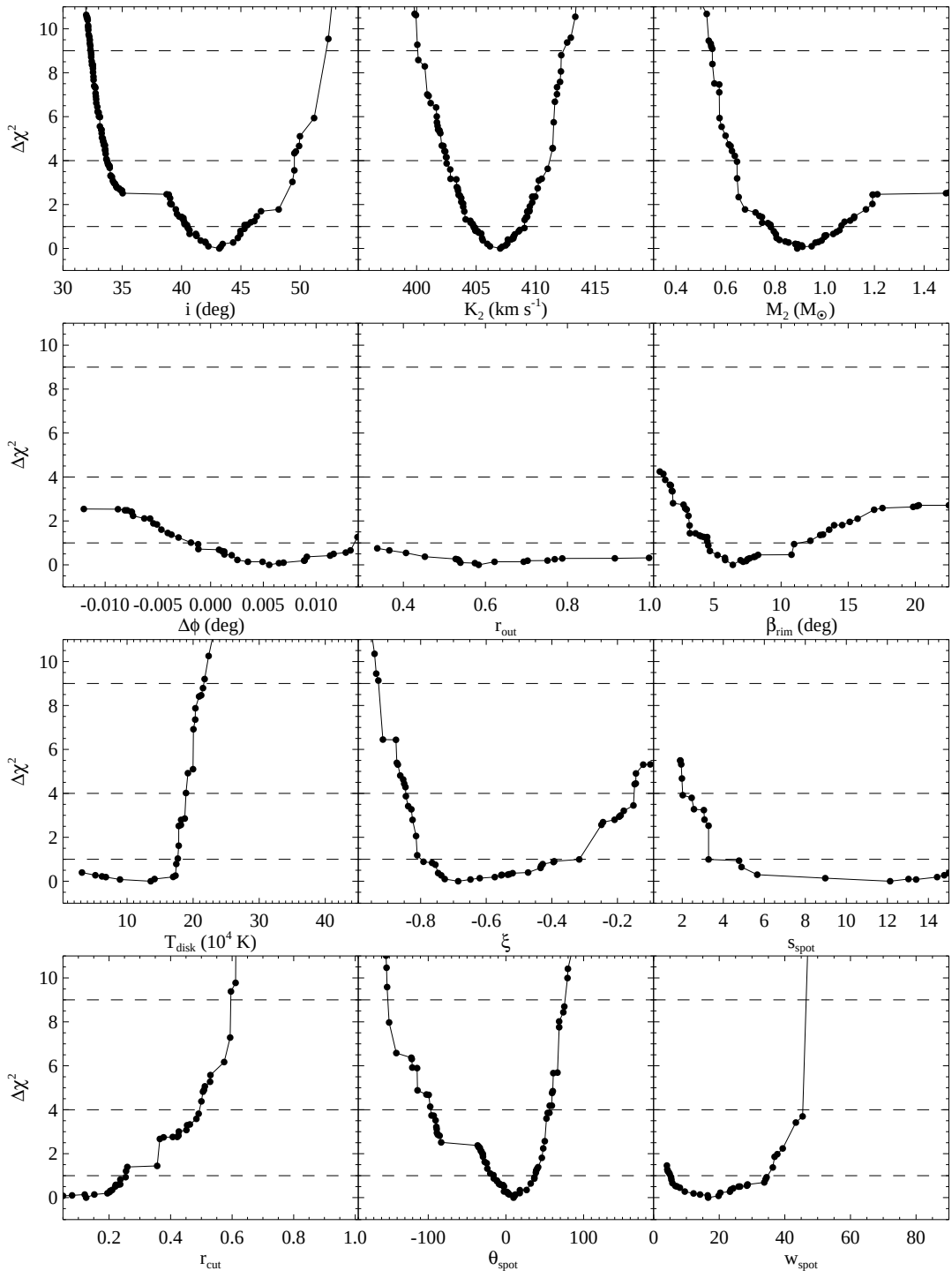

FIG. 4.— The χ^2 curves for the fit parameters. The dashed horizontal lines illustrate the 1σ, 2σ and 3σ uncertainty ranges.

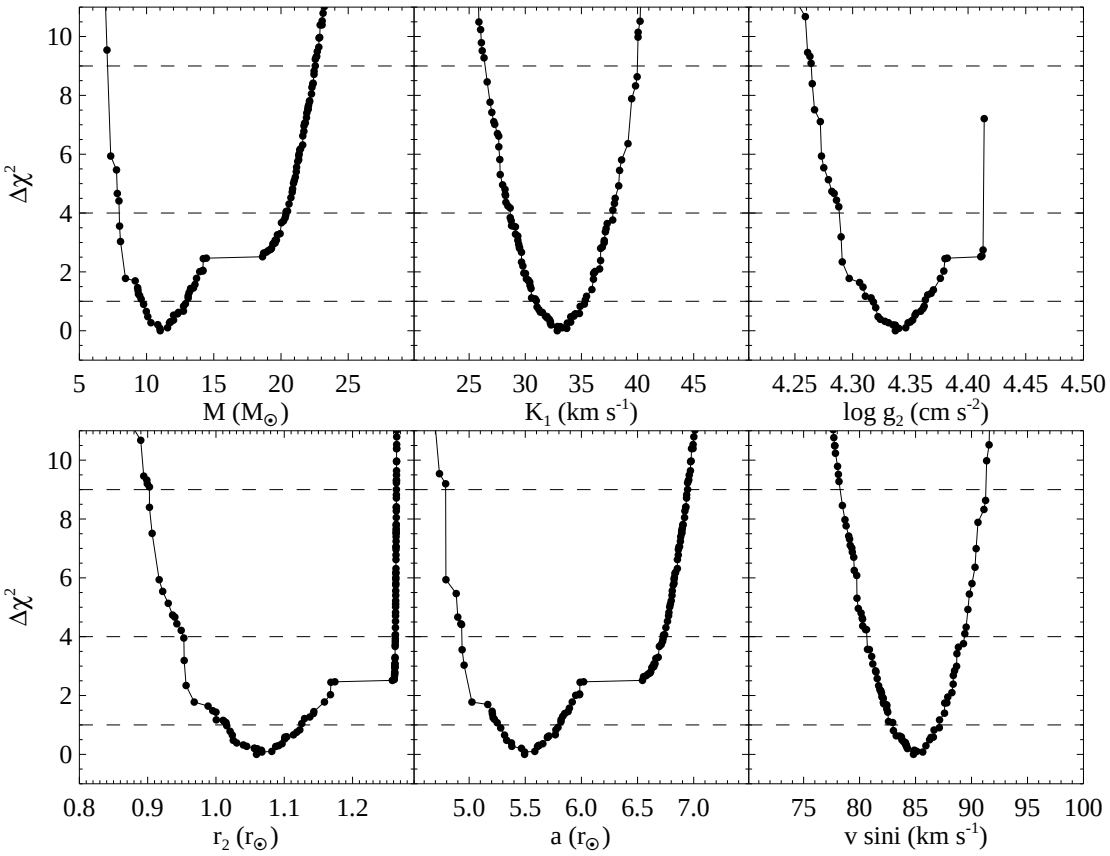

FIG. 5.— Same as Fig. 4, but for the derived parameters.

data.

An inspection of Fig. 6, which shows the model light curves decomposed into stellar and disk components, makes clear the principal virtue of the 1992 *I*-band light curve (top panel), namely, that its ellipsoidal component is minimally contaminated by the hotspot component, as well as being minimally diluted by the steady disk component. Confirmation that disk contamination was minimal during this period is provided by comparing the results of two Doppler tomographic studies: No hotspot was detected in a 1994–1995 tomogram (Casares et al. 1997), while a prominent hotspot, located where the gas stream strikes the disk, is present in a 2009–2010 tomogram (Peris et al. 2015).

Table 4 summarizes our final, key results for NovaMus. The mass of the black hole is $M = 11.0^{+2.1}_{-1.4}\,M_\odot$. The mass of the secondary star is slightly less than a solar mass ($M_2 = 0.89^{+0.18}_{-0.11}\,M_\odot$). The relation between the two masses, given our constraints on q and i, are summarized in Fig. 7. The vertical solid line on the left marks the hard lower limit on M imposed by our measurement of the mass function, and the slant solid lines show the constraints imposed by our measured values of q and i, while the dotted and dashed lines indicate 1σ errors, respectively. The gray-shaded area defines the 1σ range of uncertainty in this M–M_2 diagram. In the following section we will use the radius of the secondary ($R_2 = 1.06^{+0.07}_{-0.04}\,R_\odot$), which is essentially the solar value, to estimate the distance of NovaMus.

The black hole mass we find is significantly greater than the $M = 6.95 \pm 0.6\,M_\odot$ value reported by Gelino et al. (2001; also see Gelino 2004), which is primarily because our estimate of inclination is lower, 43.2° vs. 54°. That Gelino et al. obtained a higher inclination while ignoring the disk emission is contrary to the usual expectation because ignoring a pedestal of light causes one to underestimate the inclination (e.g., Kreidberg et al. 2012). The present case is unusual because the pedestal of light is relatively unimportant and the effect of the hotspot is dominant. Our model shows that about half the total modulation of the 2001 *J*-band light curve is due to the hot spot component (Fig. 6). Gelino et al. did not include this component and they therefore overestimated the inclination.

TABLE 4
KEY PARAMETERS FOR NOVAMUS

Parameter	Value
Mass function $f(M/M_\odot)$	3.02 ± 0.06
Mass ratio q	0.079 ± 0.007
Inclination i (deg)	$43.2^{+2.1}_{-2.7}$
Black hole mass M ($M_\odot$)	$11.0^{+2.1}_{-1.4}$
Secondary mass M_2 ($M_\odot$)	$0.89^{+0.18}_{-0.11}$
Secondary radius R_2 ($R_\odot$)	$1.06^{+0.07}_{-0.04}$
Separation a ($R_\odot$)	$5.49^{+0.32}_{-0.24}$
Distance D (kpc)	$4.95^{+0.69}_{-0.65}$

NOTE. — The quoted uncertainties are at the 1σ level of confidence.

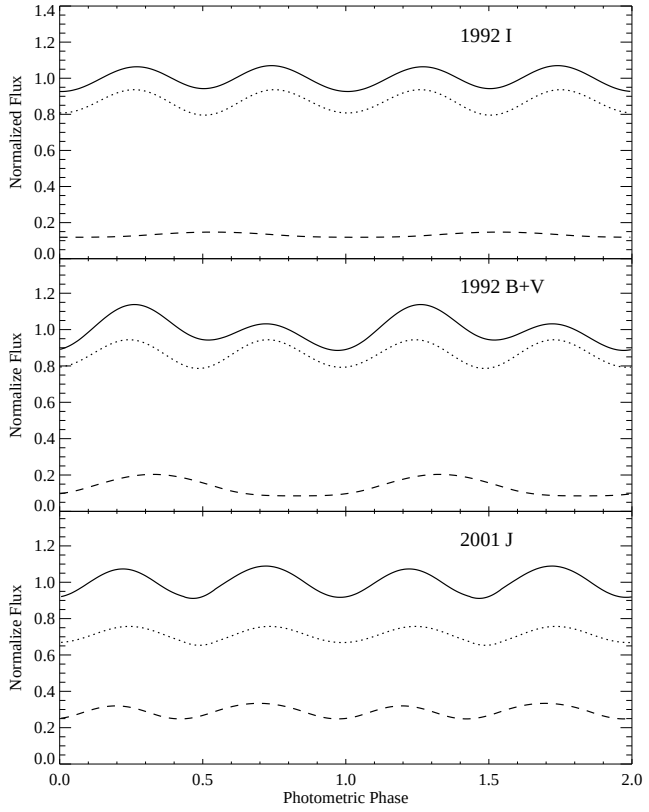

FIG. 6.— The model light curve for each filter band (solid line) shown decomposed into the stellar component (dotted line) and the disk component (dashed line). The flux is in linear units and the average level for the total model is normalized to unity. Two orbital cycles are plotted for clarity.

4. DISTANCE OF NovaMus

We follow the methodology outlined in §2 of Barret et al. (1996) to estimate the distance of NovaMus. We first determined the hypothetical absolute magnitude of the secondary star $\mathscr{M}_{\rm V}$ as viewed at its surface (i.e., at a distance $D = R_2$, rather than the canonical distance of 10 pc) using the most recent stellar atmosphere models of late-type stars. Then, using our apparent V-band magnitude corrected for reddening, and our estimate of the star's radius, we computed the distance of NovaMus.

We utilize the BT-Settl stellar atmosphere models developed by Allard et al. (2012a,b)[8]. These models provide the magnitude $\mathscr{M}_{\rm V}$ of the star at the stellar surface for a variety of filter bands over a wide grid of effective temperatures (in steps of 100 K) and surface gravities (in logarithmic steps of 0.5). For NovaMus, the effective temperature is $T_2 = 4400 \pm 100$ K (§3.1) and the surface gravity is $\log g_2 = 4.34^{+0.03}_{-0.02}$ (Table 3). Averaging the entries in the table for models in the range $\log g = 4.0 - 4.5$ with T_2 fixed at 4400 K, we find $\mathscr{M}_{\rm V} = -36.72$.

The uncertainty in $\mathscr{M}_{\rm V}$ associated with this range of $\log g$ and the 100 K uncertainty in T_2 is 0.19 mag. It is also important to assess the uncertainty in the model of Allard et al. For this purpose, we selected several stars with values of T_2 and $\log g$ close to those of the secondary for which $\mathscr{M}_{\rm V}$ can be deduced purely from observational data (Boyajian et al. 2012). The data for these stars generally agree with the models of Allard et al. to within 0.1 mag. We combine this uncertainty in quadrature with 0.19 mag to obtain the value we adopt for the absolute surface magnitude of the secondary: $\mathscr{M}_{\rm V} = -36.72 \pm 0.21$.

[8] The most recent model library is available online at https://phoenix.ens-lyon.fr/Grids/BT-Settl/CIFIST2011_2015/.

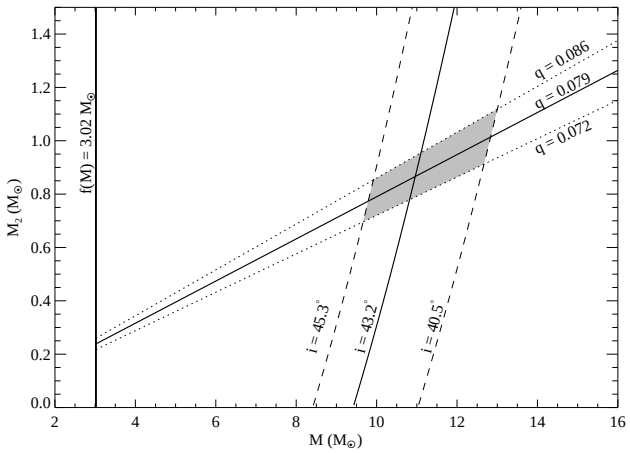

FIG. 7.— Constraints on the masses of the primary and secondary shown in the $M - M_2$ plane; the 1σ range of uncertainty is indicated by the gray-shaded region.

The apparent V-band magnitude of NovaMus is 19.85 ± 0.05 in 2009; correcting for the disk contribution $(56.7 \pm 1.4)\%$, the magnitude of the secondary alone is $m_{\rm V} = 20.76 \pm 0.06$. Next, we correct for reddening, relying on two observations of the 2200 Å dust feature in the ultraviolet spectrum of NovaMus. Cheng et al. (1992) reported $E(B-V) = 0.287 \pm 0.004$ based on observations made using the Faint Object Spectrograph (FOS) onboard the *Hubble Space Telescope*, while Shrader & Gonzalez-Riestra (1993) obtained a consistent result, $E(B-V) = 0.30 \pm 0.05$ based on observations made using the *International Ultraviolet Explorer*. We take $E(B-V) = 0.29 \pm 0.05$, adopting the larger error bar to cover the uncertainty in converting $E(B-V)$ to $A_{\rm V}$ using the standard extinction law: $A_V = R(V) \times E(B-V)$ with $R(V) = 3.1$ (Cardelli et al. 1989). We therefore conclude that the reddening of NovaMus is $A_{\rm V} = 0.90 \pm 0.16$ and the dereddened V-band magnitude of the secondary is $m_{\rm V_0} = 19.86 \pm 0.17$.

The distance D can then be obtained from the equation

$$5 \log(D/R_2) = m_{\rm V_0} - \mathscr{M}_{\rm V} = 56.58 \pm 0.27, \qquad (2)$$

where $R_2 = 1.06^{+0.07}_{-0.04}\ R_\odot$ is the radius of the secondary (§3.2). We therefore conclude that the distance of NovaMus is $D = 4.95^{+0.69}_{-0.65}$ kpc. This value is consistent with most literature estimates, which are generally based on the methodology we employ; e.g., 5.1 kpc (Gelino et al. 2001), 5.0 ± 1.0 kpc (Esin et al. 1997), 5.5 ± 1.0 kpc (Orosz et al. 1996), and > 4 kpc (King et al. 1996). Using NIR photometric data, while ignoring the disk contribution, Shahbaz et al. (1997) obtained a lower estimate of $D = 2.8$–4.0 kpc.

5. SUMMARY & DISCUSSION

Combining the various results presented herein with those in Paper I, we have obtained three principal results:

1. We present the first evidence that BHSXTs brighten

gradually and steadily between outburst cycles. For NovaMus, SMARTS data show the rate to be 0.0357 ± 0.0006 mag yr^{-1} in the V-band and 0.0199 ± 0.0004 mag yr^{-1} in the I-band for the period 2003 to 2015 (sans 2010). Between the time NovaMus returned to quiescence following its 1991 outburst and today, the total brightening in the V-band is ≈ 0.8 mag. This result provides support for the disk instability model and the work of Cantrell et al. (2008, 2010) on optical states and state changes. It also underscores the importance of obtaining light curve data early in the quiescent phase for use in constraining the systemic inclination via ellipsoidal modeling.

2. By modeling three archival optical/NIR light curves of the highest quality using the ELC code, we determined the systemic inclination of NovaMus to be $i = 43.2^{+2.1}_{-2.7}$ deg. Our measured value of the black hole mass is $M = 11.0^{+2.1}_{-1.4}\ M_{\odot}$, while the mass of the secondary is $M_2 = 0.89^{+0.18}_{-0.11}\ M_{\odot}$.

3. Based on our determination of the radius of the secondary, $R_2 = 1.06^{+0.07}_{-0.04}\ R_{\odot}$, we estimate the distance of NovaMus to be $D = 4.95^{+0.69}_{-0.65}$ kpc. We will use this estimate of D, along with our estimates of i and M, archival X-ray data, and the continuum-fitting method to estimate the spin of the black hole, a result that will be presented in a companion paper (Chen et al. 2015).

Among transient X-ray sources, the black hole mass in NovaMus is high, deviating by $\sim 3\sigma$ from the narrowly-distributed mass distribution of BHSXTs centered at $7.8 \pm 1.2\ M_{\odot}$ (Özel et al. 2010; Farr et al. 2011; McClintock et al. 2014). The two rivals are the black holes in GRS 1915+105 ($M = 12.4^{+2.0}_{-1.8}\ M_{\odot}$; Reid et al. 2014) and in GS 2023+338 ($M = 12 \pm 2 M_{\odot}$; Charles & Coe 2006; but see Khargharia et al. 2010). The general lack of massive black holes among BHSXTs can be explained by the evolutionary paths of low-mass X-ray binaries during which the star loses substantial mass before the supernova explosion (Özel et al. 2010). The black hole in NovaMus may be spinning relatively rapidly as the result of accretion torques, if the black hole's birth mass is significantly less than the current mass (Fragos & McClintock 2015).

We note three lessons learned for future attempts to obtain robust measurements of the masses of black holes in BHSXTs based on our results and on the results of earlier studies (e.g., Cantrell et al. 2008, 2010; Kreidberg et al. 2012): 1) perform the spectroscopic and photometric monitoring observations simultaneously in order to accurately correct for disk emission; 2) use only passive-state light curve data for which the non-stellar emission is free of strong flickering and can be well-modeled by a steady disk component plus a hotspot component; and 3) obtain optical monitoring data soon after the system returns to quiescence, when the disk emission is minimal.

Concerning the first of the three points – the need for simultaneity – this is particularly important for short-period systems because the disk component is often dominant. Furthermore, as an inspection of Fig. 1 makes clear, this component not only varies from season to season, but it varies on much shorter timescales as well. The key methodology we employed was insuring that our spectroscopic and photometric data were obtained strictly simultaneously. Although the V-band light curve we obtained in 2009 was unsuitable for ellipsoidal modeling because the system was in the active state, we were nevertheless able to use it (and the spectroscopic data) to very precisely constrain the disk fraction for our selected archival light curves (§2.3).

In closing, we comment briefly on ellipsoidal studies of short-period BHSXTs by other groups (see also Kreidberg et al. 2012). Cantrell et al. (2010) obtained robust estimates of i and M for A0620−00 using nearly simultaneous spectroscopic and photometric data to constrain the disk fraction. Khargharia et al. (2013) likewise obtained high-quality constraints on i and M for XTE J1118+480 based on NIR photometry and spectroscopy performed on the same night. GS 2000+25 appears to be a very favorable system; the disk fraction is minimal, and the orbital modulation almost purely ellipsoidal. However, Ioannou et al. (2004) report relatively weak constraints on i and M because the disk fraction and the mass ratio q were poorly constrained. For XTE J1859+226, Corral-Santana et al. (2011) obtained passive-state light curves, but their disk fraction is poorly constrained because two years elapsed between their photometric and spectroscopic observations. The light curves of GRO J0422+32 are always observed to be dominated by aperiodic flickering; Reynolds et al. (2007) conclude that attempts to constrain the mass of the black hole are "prone to considerable uncertainty" because of the contaminating effects of disk emission. In conclusion, one must be cautious of masses published for short-period BHSXTs based on non-simultaneous photometry and spectroscopy, and doubly cautious of studies that ignore the disk emission altogether (e.g. Gelino & Harrison 2003).

We thank D. Steeghs, P. Longa-Peña, P. J. Callanan, L. C. Ho, P. G. Jonker, M. T. Reynolds, and M. A. P. Torres for their contributions to this work, which are reported in Paper I. L.J.G acknowledges the support of the Chinese Academy of Sciences through grant No. XDB09000000 (Emergence of Cosmological Structures) from the Strategic Priority Research Program; of the National Natural Science Foundation of China (grant No. 11333005); and of the National Astronomical Observatories of China (grant No. Y234031001).

REFERENCES

Allard, F., Homeier, D., & Freytag, B. 2012a, Royal Society of London Philosophical Transactions Series A, 370, 2765
Allard, F., Homeier, D., Freytag, B., & Sharp, C. M. 2012b, in EAS Publications Series, Vol. 57, EAS Publications Series, ed. C. Reylé, C. Charbonnel, & M. Schultheis, 3–43
Barret, D., McClintock, J. E., & Grindlay, J. E. 1996, ApJ, 473, 963
Beer, M. E., & Podsiadlowski, P. 2002, MNRAS, 331, 351
Belczynski, K., Wiktorowicz, G., Fryer, C. L., Holz, D. E., & Kalogera, V. 2012, ApJ, 757, 91
Boyajian, T. S., von Braun, K., van Belle, G., et al. 2012, ApJ, 757, 112
Cantrell, A. G., Bailyn, C. D., McClintock, J. E., & Orosz, J. A. 2008, ApJ, 673, L159
Cantrell, A. G., Bailyn, C. D., Orosz, J. A., et al. 2010, ApJ, 710, 1127
Cardelli, J. A., Clayton, G. C., & Mathis, J. S. 1989, ApJ, 345, 245
Casares, J., & Jonker, P. G. 2014, Space Sci. Rev., 183, 223
Casares, J., Martín, E. L., Charles, P. A., Molaro, P., & Rebolo, R. 1997, New A, 1, 299
Charles, P. A., & Coe, M. J. 2006, Optical, ultraviolet and infrared observations of X-ray binaries, ed. W. H. G. Lewin & M. van der Klis, 215–265

Chen, Z., Gou, L., McClintock, J. E., et al. 2015, ApJ, submitted
Cheng, F. H., Horne, K., Panagia, N., et al. 1992, ApJ, 397, 664
Corral-Santana, J. M., Casares, J., Shahbaz, T., et al. 2011, MNRAS, 413, L15
Dubus, G., Hameury, J.-M., & Lasota, J.-P. 2001, A&A, 373, 251
Eggleton, P. P. 1983, ApJ, 268, 368
Esin, A. A., McClintock, J. E., & Narayan, R. 1997, ApJ, 489, 865
Farr, W. M., Sravan, N., Cantrell, A., et al. 2011, ApJ, 741, 103
Fender, R. P., Gallo, E., & Russell, D. 2010, MNRAS, 406, 1425
Fender, R. P., Garrington, S. T., McKay, D. J., et al. 1999, MNRAS, 304, 865
Fragos, T., & McClintock, J. E. 2015, ApJ, 800, 17
Fryer, C. L., & Kalogera, V. 2001, ApJ, 554, 548
Gelino, D. M. 2004, in Revista Mexicana de Astronomia y Astrofisica, vol. 27, Vol. 20, Revista Mexicana de Astronomia y Astrofisica Conference Series, ed. G. Tovmassian & E. Sion, 214–214
Gelino, D. M., & Harrison, T. E. 2003, ApJ, 599, 1254
Gelino, D. M., Harrison, T. E., & McNamara, B. J. 2001, AJ, 122, 971
Greene, J., Bailyn, C. D., & Orosz, J. A. 2001, ApJ, 554, 1290
Ioannou, Z., Robinson, E. L., Welsh, W. F., & Haswell, C. A. 2004, AJ, 127, 481
Khargharia, J., Froning, C. S., & Robinson, E. L. 2010, ApJ, 716, 1105
Khargharia, J., Froning, C. S., Robinson, E. L., & Gelino, D. M. 2013, AJ, 145, 21
King, N. L., Harrison, T. E., & McNamara, B. J. 1996, AJ, 111, 1675
Kochanek, C. S. 2014, ApJ, 785, 28
Kreidberg, L., Bailyn, C. D., Farr, W. M., & Kalogera, V. 2012, ApJ, 757, 36
Lasota, J.-P. 2001, New A Rev., 45, 449
Marshall, J. L., Burles, S., Thompson, I. B., et al. 2008, in Society of Photo-Optical Instrumentation Engineers (SPIE) Conference Series, Vol. 7014, Society of Photo-Optical Instrumentation Engineers (SPIE) Conference Series, 54
McClintock, J. E., Narayan, R., & Steiner, J. F. 2014, Space Sci. Rev., 183, 295
Morningstar, W. R., Miller, J. M., Reis, R. C., & Ebisawa, K. 2014, ApJ, 784, L18
Narayan, R., & McClintock, J. E. 2005, ApJ, 623, 1017
—. 2012, MNRAS, 419, L69
Narayan, R., McClintock, J. E., & Tchekhovskoy, A. 2014, Energy Extraction from Spinning Black Holes Via Relativistic Jets, ed. J. Bičák & T. Ledvinka, 523
Narayan, R., & Yi, I. 1994, ApJ, 428, L13
Orosz, J. A., & Bailyn, C. D. 1997, ApJ, 477, 876
Orosz, J. A., Bailyn, C. D., McClintock, J. E., & Remillard, R. A. 1996, ApJ, 468, 380
Orosz, J. A., & Hauschildt, P. H. 2000, A&A, 364, 265
Orosz, J. A., Steiner, J. F., McClintock, J. E., et al. 2014, ApJ, 794, 154
Özel, F., Psaltis, D., Narayan, R., & McClintock, J. E. 2010, ApJ, 725, 1918
Peris, C. S., Vrtilek, S. D., Steiner, J. F., et al. 2015, MNRAS, 449, 1584
Reid, M. J., McClintock, J. E., Steiner, J. F., et al. 2014, ApJ, 796, 2
Remillard, R. A., & McClintock, J. E. 2006, ARA&A, 44, 49
Remillard, R. A., McClintock, J. E., & Bailyn, C. D. 1992, ApJ, 399, L145
Reynolds, M. T., Callanan, P. J., & Filippenko, A. V. 2007, MNRAS, 374, 657
Reynolds, M. T., Callanan, P. J., Robinson, E. L., & Froning, C. S. 2008, MNRAS, 387, 788
Russell, D. M., Gallo, E., & Fender, R. P. 2013, MNRAS, 431, 405
Shahbaz, T., Naylor, T., & Charles, P. A. 1997, MNRAS, 285, 607
Shrader, C. R., & Gonzalez-Riestra, R. 1993, A&A, 276, 373
Steiner, J. F., & McClintock, J. E. 2012, ApJ, 745, 136
Steiner, J. F., McClintock, J. E., & Narayan, R. 2013, ApJ, 762, 104
Steiner, J. F., McClintock, J. E., & Reid, M. J. 2012, ApJ, 745, L7
Sutaria, F. K., Kolb, U., Charles, P., et al. 2002, A&A, 391, 993
van der Hooft, F., Heemskerk, M. H. M., Alberts, F., & van Paradijs, J. 1998, A&A, 329, 538
Wu, J., Orosz, J. A., McClintock, J. E., et al. 2015, ApJ, 806, 92